Journal of Structural Geology 32 (2010) 1085–1100

Contents lists available at ScienceDirect

Journal of Structural Geology

journal homepage: www.elsevier.com/locate/jsg

Tip to midpoint observations on syntectonic veins, Ouachita orogen, Arkansas: Trading space for time

Pablo Cervantes [1], David V. Wiltschko*

Texas A&M University, Center for Tectonophysics, Department of Geology and Geophysics, Spence Street, College Station, TX 77843-3115, United States

ARTICLE INFO

Article history:
Received 25 November 2008
Received in revised form
22 June 2010
Accepted 24 June 2010
Available online 14 July 2010

Keywords:
Veins
Veinlets
Fracture
Fracturing
Boudinage
Boudins
Ouachitas
Mazarn shale
Benton uplift
Arkansas

ABSTRACT

By examining a vein from its tip to center, we have established the transition from a single filled fracture at the vein tip to typical 'crack-seal' textures observed in fibered, laminated veins. The vein is contained in the boudin neck of a sandstone layer within the Lower Ordovician Mazarn Formation, Benton Uplift, Ouachita orogen. The tip of the vein is composed of one or more isolated veinlets, defined as quartz-filled narrow (5–25 μm) fractures parallel to the larger vein's long dimension. Scanned SEM-based cathodoluminescence shows that quartz laminae of the same orientation and thickness are found throughout the vein. Wall-normal fibers first appear in the vein where detrital grains are cut by multiple veinlets, each veinlet mimicking the crystallographic orientation of the detrital grain, whereas later veinlets reflect the established crystallographic orientation of the fiber. Fibers throughout the vein retain evidence of having been formed by repeated fracturing and filling of a pre-existing grain (at the vein walls) or fiber. However, recrystallization later modified the fibers by obliterating some evidence of the veinlets and moving fiber walls. Boudin formation provided the extension site that localized fracturing and vein filling. The vein grows by the repeated addition of veinlets in the neck region. Recrystallization altered the shape of previously formed fibers.

1. Introduction

Despite a wealth of observations on syntectonic veins from a variety of tectonic regimes, fundamental questions remain as to the interplay of fracturing and vein filling. For example, although the origin of veins as fractures is largely established (e.g., Ramsay, 1980; Cox, 1987; Fisher and Brantley, 1992; Bons, 2000; and Hilgers and Urai, 2002; Laubach et al., 2004a), it's not always clear why fractures initiate where they do and how the vein propagates once started. For sample, is fracture initiation followed immediately by fracture-filling or is the processes of precipitation in part responsible for the fracture initiating (e.g., Taber, 1916, 1918 and 1920; Misik, 1971; Li, 2000; Means and Li, 2001; Wiltschko and Morse, 2001). In those fractures that show "crack-seal" textures or vein-parallel bands of precipitate, what controls the localization of repeated fracturing? How do wall-normal fibers develop by wall-parallel fracturing? What role does cementation have in altering the mechanics of fracture propagation as the vein grows?

The problem of understanding the evolution of veins is in part one of scale. Veins that are meters long may be made up of grains that are microns in size, a range of 6 orders of magnitude. To date, fabric observations have been largely confined to small portions of veins, usually their centers (although see Laubach et al., 2004b). This approach has not yielded the observations directly applicable to the initiation of vein fabrics. In this paper, we report on a study of a vein from tip to midpoint in order to trace the evolution of vein formation from initiation to appreciable aperture. By choosing a vein that is of moderate length yet representative of fibered veins, our purpose is to trace the textures from tip to midpoint to understand the transition from a single fracture to a well-developed fibered, banded "crack-seal" vein. Our idea is that if the tip represents the earliest stages of vein formation and the midpoint the most advanced stage that a particular vein displays, then one can observe the progression of fabric development. Therefore, this paper is an exercise in examining the evolution of a single vein from tip to center under the assumption that it is possible to trade space for time, although how much time is not known. With this assumption, we can begin to answer some of the questions raised above.

The vein sampled for this study came from the Ouachita Mountains in Arkansas. This vein is typical in that it is fibrous and shows "crack-seal" textures or banding parallel to the vein wall.

* Corresponding author.
E-mail addresses: pablo.cervantes@bp.com (P. Cervantes), d.wiltschko@tamu.edu (D.V. Wiltschko).
[1] Present address: BP America, Inc.

0191-8141/$ – see front matter © 2010 Elsevier Ltd. All rights reserved.
doi:10.1016/j.jsg.2010.06.017

2. Geological setting

The veins of interest are found in the Benton Uplift of the Ouachita fold and thrust belt. The latter orogenic belt trends east–west and extends from central Arkansas to southeastern Oklahoma (Fig. 1A). To the east, the Ouachita system plunges beneath Mesozoic and Tertiary sediments of the Mississippi embayment. Based on COCORP reflection profiles, Lillie et al. (1983) and Nelson et al. (1982) proposed that during the lower Paleozoic the area was a south facing passive continental margin followed in the Mississippian by collision with a southern, unknown block with North America. A thick Carboniferous marine shale facies at least 12 km thick (e.g., Houseknecht and Matthews, 1985) was emplaced on coeval shelf carbonates. Late motion on a crustal-scale ramp resulted in the northward and vertical movement of a portion of the continental margin producing the Benton and Broken Bow uplifts (Fig. 1A).

The frontal portion of the Ouachitas consist of north to northwest verging folds and thrusts faults, although in places the most exterior structure is a triangle zone (e.g., Arbenz, 1989). Uplift of the core of the orogen (Broken Bow and Benton uplifts) has resulted in south-vergent folds and north-dipping cleavage on the south flank of the core. The deeper structures causing the core uplift displace margin sediments and/or continental crust on thrusts that most likely crop out at the thrust front. This deep thrusting was a late event because sediments are continuous both north and south of the uplifts until late Pennsylvanian or earliest Permian.

Paleo-thermal gradients, while cut by thrust faults, are lower than would be predicted from burial of each thrusted sequence suggesting that thrusting was synchronous with peak metamorphism (Underwood et al., 1988). Vitrinite reflectance values increase to the southeast, leading Houseknecht and Matthews (1985) to suggest that postorogenic Cretaceous plutons influenced the thermal maturation of the core of the orogen. However,

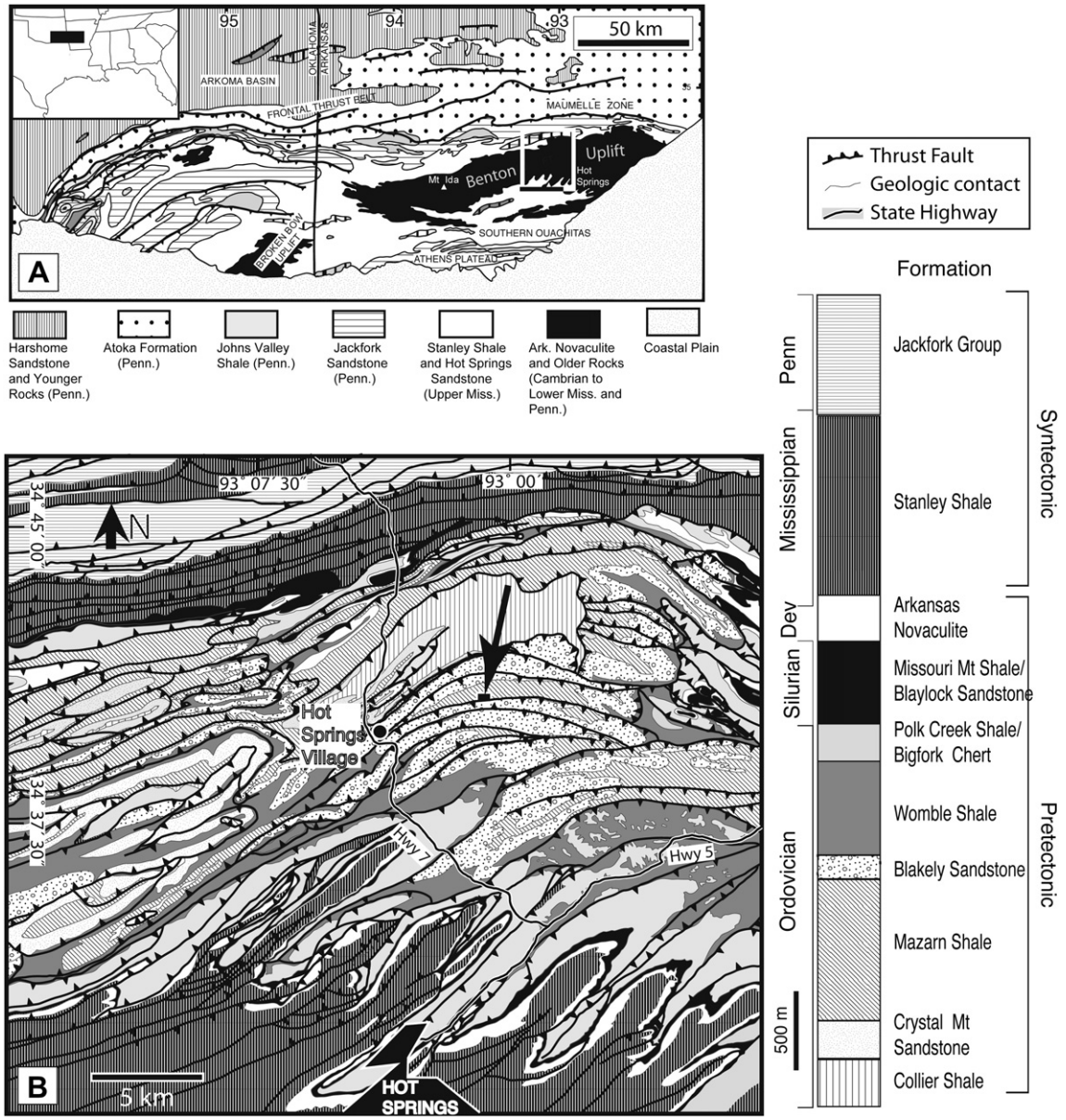

Fig. 1. Geologic map of the Ouachitas. (A) Geologic map of the Ouachitas after Miser (1959). The white square shows the location of the Hot Springs area. (B) Regional geology of the Hot Springs, AR, area with the location of the Lake Pineda dam outcrop (black arrow pointing to solid black rectangle). After Haley and Stone (1996).

apatite fission-track analysis results show that regional cooling of the Ouachitas took place in Late Paleozoic, before emplacement of post-tectonic Cretaceous plutons within the Mississippi Embayment (Arne, 1992). Two proposals for the origin of the Cretaceous apatite fission-track ages are passage of the Bermuda hotspot (Cox and Van Arsdale, 1997, 2002) and postorogenic burial followed by Cretaceous exhumation (Corrigan et al., 1998).

The greatest concentration of quartz veins in the Ouachitas is found in a region 50–65 km wide at the center of the Benton and Broken Bow Uplifts (Miser, 1959). The rocks containing veins are also the rocks with highest metamorphic grade. The central part of the Benton Uplift is characterized by both north-dipping thrust faults and south-verging overturned folds (Fig. 1B). Miser (1959) observed that the veins in this region follow faults, bedding planes and fractures with the latter cutting across folds. The structural setting of the veins in the Ouachitas suggests that the veins are synorogenic (Nielsen et al., 1989; Viele, 1989). Radiometric dating of adularia in commercial quartz veins yield Late Pennsylvanian to Early Permian ages (Bass and Ferrara, 1969; Denison et al., 1977; Shelton et al., 1986).

3. Outcrop geology

All samples come from an outcrop located at Hot Springs Village, 13 miles north of Hot Springs, AK (Stone et al., 1994). The rocks exposed at the outcrop are from the Lower Ordovician Mazarn Shale, an interbedded banded green and black shale, laminated fine-grained gray siltstone, and minor lenses of fine-grained brownish-gray quartzitic sandstone. This formation has been interpreted to have been deposited as density and marine currents from north or northeast sources (Stone and McFarland, 1981; Lowe, 1989).

These rocks were deformed and metamorphosed up to greenschist facies as part of the Benton uplift. The outcrop is crossed by two thrust faults oriented N60E (Fig. 2). Fold wavelengths vary from cm's to m's in length. Small (cm to dm) folded sandstone layers are contained within shale beds while larger wavelength folds involve thicker (dm to m) sandstone beds. All shale units display cleavage in outcrop whereas the sandstone units do not.

Bedding (Fig. 3A) strikes NE–SW. Fold axes (Fig. 3B) are consistent with those observed in other areas of the Benton uplift, namely NE–SW trending axes as reported by Viele (1973). Fold axes and bedding orientations are consistent with NW–SE contraction. Cleavage (Fig. 3C) is subhorizontal and at a low angle to bedding, indicating subvertical flattening. Joints (Fig. 3E) show two orthogonal sets. Joints cut across all features in the outcrop. Thrust faults both cut through folds and parallel fold axial surfaces.

Veins (Fig. 3D) are either subvertical or subhorizontal. The veins described come from the vertical sets. Vein aspect ratios in outcrop are bimodal. The *low-aspect ratio* veins are thin and elongated in shape and range between 0.1 and 1 m long and between 1 mm and 4 mm wide. The *high-aspect ratio* veins range between 30 cm and 5 m long and 5 cm and 40 cm wide. All veins are both fibered and bi-mineralic with quartz and less common calcite fibers. In hand sample, cross-cutting relationships show that veins are earlier than faults and apparently later than cleavage formation since cleavage cannot be traced across veins. However, it is difficult to trace cleavage through a pure quartz-calcite vein. The relative timing of the calcite and quartz in the vein is not known definitively. Some but not all of the calcite grains contain mechanical e-twins and many are intimately intergrown with quartz. However, there are also calcite grains that adjoin rare open space in the vein and display small (<5 μm) crystal terminations jutting into that space. The timing of these terminated crystals is not known.

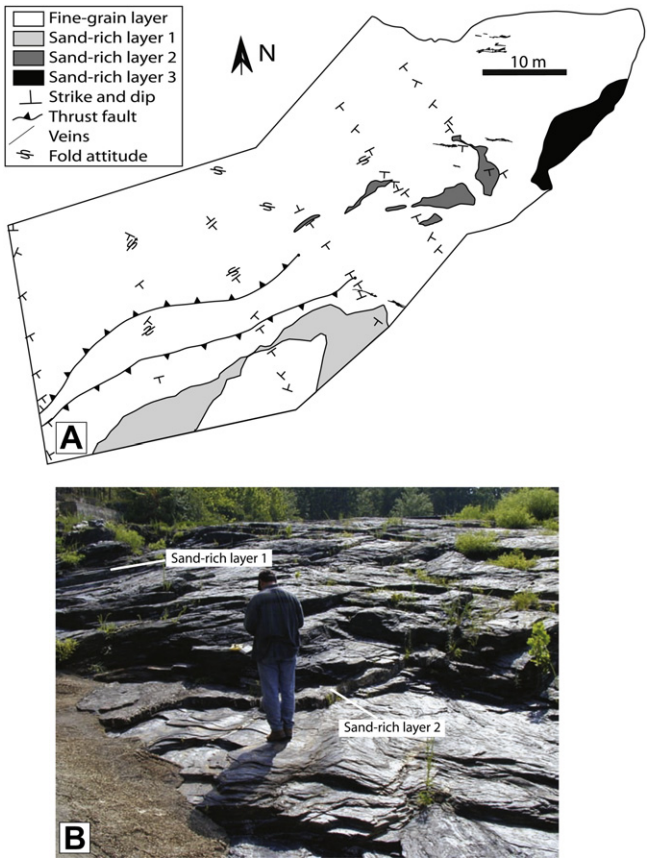

Fig. 2. Lake Pineda dam outcrop geology. (A) Map of the outcrop. (B) Photo of the outcrop.

Sandstone beds in the outcrop are boudinaged (Fig. 4A and B). The boudins are symmetrical 'drawn boudins' by the classifications of Goscombe et al. (2004). High-aspect ratio veins are located at the boudin necks. The fact that veins preferentially are located in the necks of boudins suggests that these boudins also have characteristics of what Goscombe et al. (2004) term 'torn boudins.' Whereas all of the high-aspect veins we observed occur in boudin necks, many but not all or the low-aspect veins do so. The particular vein that we studied is in a boudin neck. The linear correlation between bed thickness and separation between boudin necks where the veins are located supports the mechanical link between boudinage and veins (Fig. 4C). The orientation of boudin necks (boudin axes) corresponds to the largest concentration of vein orientations NW–SE (Fig. 3F).

P-T condition of vein formation determined from fluid inclusions and quartz-calcite oxygen isotopes thermometry is between 275 and 385 °C and 1100 and 3400 bars (Cervantes, 2007).

4. Vein textures

The vein we studied is 62 cm long, up to 5 mm wide and, a low-aspect ratio vein in this outcrop. Its midline is oriented N75W and the vein walls are both vertical and bed normal. The depth of the vein into the outcrop is unknown but from the sample obtained is at least 1 cm. The vein is fibrous throughout its length with quartz and calcite fibers and some apatite grains (Fig. 5).

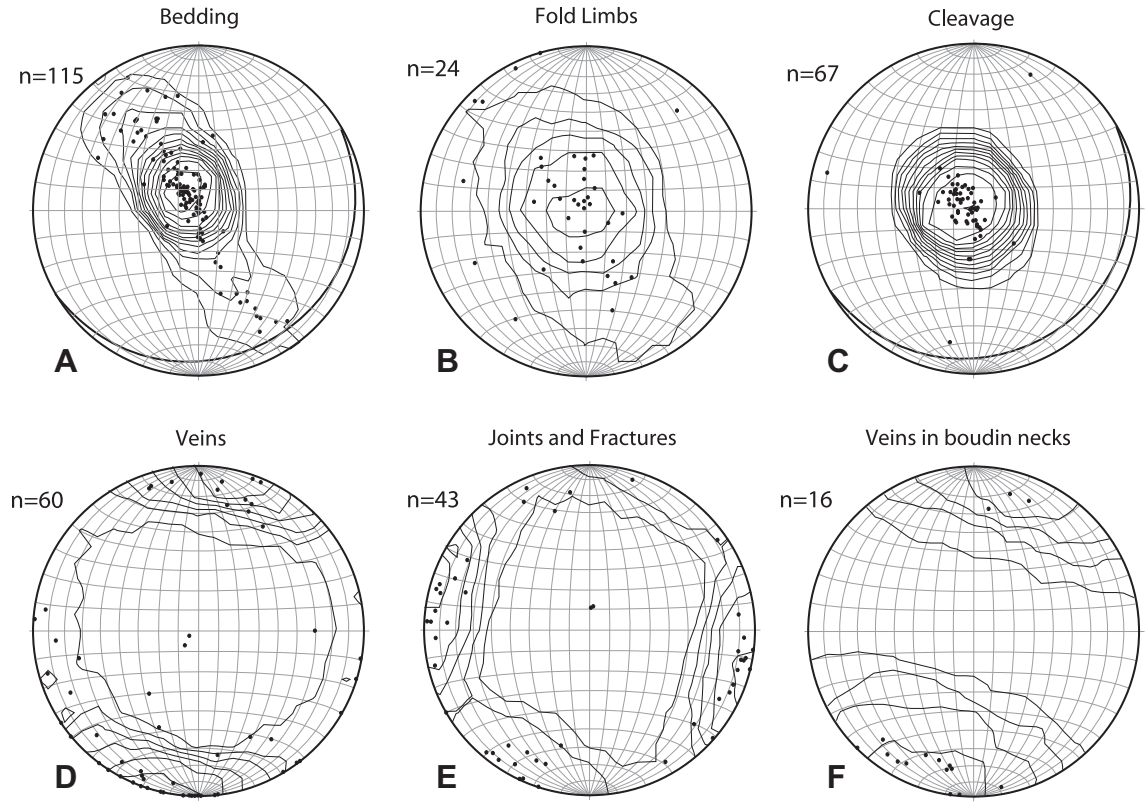

Fig. 3. Structural data from Lake Pineda dam outcrop. All figures are lower hemisphere, equal area projections. All contours are Kamb contours with $\sigma = 2.0$. (A) Poles to bedding planes from the entire outcrop. The bold great circle represents the orientation of the main thrust fault in the outcrop. (B) Poles to bedding (fold limbs) from small folds in the outcrop. (C) Poles to cleavage planes of the entire outcrop. Great circle represents the orientation of the main thrust fault. (D) Poles to vein orientations. (E) Poles to joint orientations. (F) Poles to orientations of veins in boudin necks.

We documented vein and host textures using petrographic microscopes, electronic microprobe X-ray element maps and SEM-based or scanned cathodoluminescence (SEM-CL). SEM-CL has been used effectively to document textures not discernible by other techniques including transmitted light, backscattered electron (BSE) or even optical (cold cathode) CL microscopy (Pagel et al., 2000; Gotze et al., 2001; Milliken and Laubach, 2000; Bignall et al., 2004). The SEM-CL method offers high spatial resolution and a wide range of acceleration voltages making it useful for both calcite and minerals with weak luminescence such as quartz.

The instrument at the Texas A&M Microscopy and Imaging Center is a FEI Quanta 600 FE-SEM equipped with a Gatan panchromatic cathodoluminescence detector with RGB filters. False-color composite images may be constructed by acquiring one image each with each filter and then combining or stacking them in photo editing software. As there is no color calibration, these images were constructed to yield the most textural information. Due to the persistent luminescence of carbonate minerals (Reed and Milliken, 2003), the gain on the detector had to be reduced with the red filter in place compared to the images acquired with the green or blue filters. For the same reason, beam dwell time was reduced such that image acquisition was typically several minutes. In exceptional cases, image acquisition was up to 10 min in order to minimize streaking due to persistent luminescence. The operating voltage was 15 kV.

4.1. Host

The host consists of interbedded layers cm to m thick and laminations mm to cm thick of both fine-grained (silt to clay size) and coarse-grained (medium sand to silt size) material. Veins in the outcrop are best exposed along, and are normal to, slip surfaces. These slip surfaces are observed on bedding planes of the thicker (dm to m thick) layers of sandstone and are indicated by slickenlines, enhanced polish and occasional mineral fibers.

Electron-microprobe X-ray maps obtained from different areas of various thin sections, combined with XRD analyses of both coarse-grain and fine-grain host fractions, were used to determine that the mineralogy of the coarse-grained host is mostly quartz (>75% by area on X-ray maps) with varying amounts of clay minerals (illite), chlorite, and traces of other minerals such as apatite, calcite and feldspars (Cervantes, 2007). The mineralogy of the fine-grained host is similar but clay minerals and chlorite are more abundant than quartz (<45% by area on the X-ray maps).

Composite SEM-CL images show that (1) host quartz luminescence is different from that of the vein quartz, and (2) the difference in luminescence between quartz in the host and the veins shows clear evidence of host grains fractured and displaced by vein mineralization (Fig. 6A and C).

Microscopically, host cleavage is delineated by dark linear bands 5–30 μm thick where the host rock is devoid of quartz. In addition, phyllosilicates are concentrated in cleavage zones in comparison to the concentration of these minerals in the surrounding host. Quartz appears to be preferentially removed in these zones.

4.2. Veinlets

A nearly ubiquitous feature of this vein is the preservation of veinlets. Veinlets are defined in this paper as thin (5–25 μm) veins parallel or at low angles to those portions of the host–vein interface

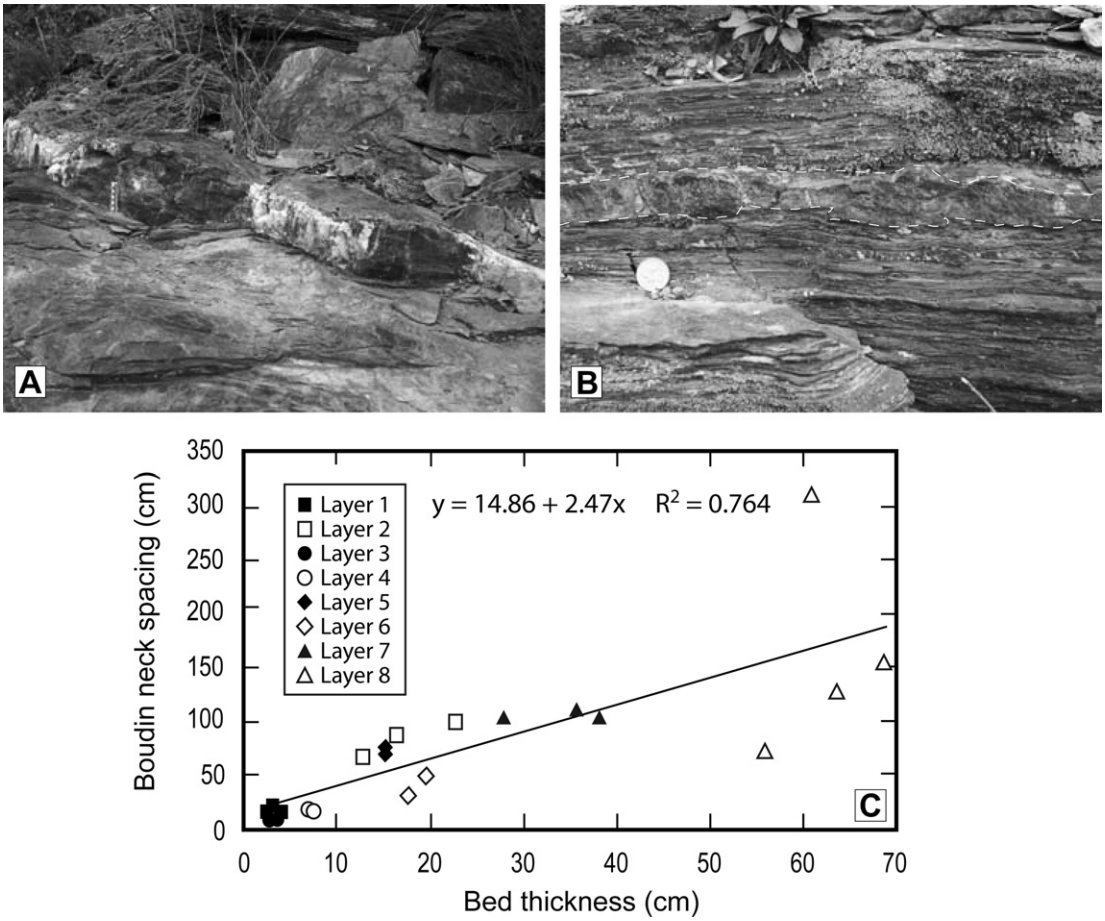

Fig. 4. Boudinage at Pineda Dam Outcrop. (A) Boudinage in a thick sandstone layer (30.5 cm). Scale in the photo represents 10 cm. (B) Boudinage in a thin sandstone layer (3.81 cm) outlined with dotted white line on photo. A quarter dollar is shown for scale. (C) Plot of bed thickness vs. separation of boudin necks. These features show a linear correlation described by the line shown with $R^2 = 0.76$.

that contain quartz (Fig. 6; see also Fig. 8). Veinlets have the same mineralogy as the larger vein. The fill of many veinlets, especially toward their distal ends, is one crystal wide. Veinlets can be found next to one another or separated by host segments up to 15–30 μm wide. The host segments have the same mineralogy and texture as the host adjacent to the vein (Fig. 6A, B and E). Veinlets are more abundant close to the tip where they represent 100% of the total vein width whereas near the widest part of the vein they represent approximately 5% of the total vein width.

Veinlets are present along the entire length of the vein, regardless of host grain size (Figs. 6–8, and 9). False-color SEM-CL images show that luminescence color differs between: (1) quartz in veinlets, (2) quartz in the main body of the vein, and (3) quartz in the host. Color differences indicate variations in trace element chemistry of the quartz (Hervig and Peacock, 1989; Perny et al., 1992; Watt et al., 1997; Monecke et al., 2002) but those differences are not resolvable by microprobe analysis in our samples. Quartz in veinlets luminesces blue, quartz in fibers along the main body of the vein luminesces pink, while quartz in the host luminesces from light blue to green (Figs. 6 and 9). SEM-CL shows sharp boundaries between grains inside some veinlets, in which interpret these sharp contacts as being euhedral terminations (Fig. 6C).

4.3. Fibers

Fibers are elongated strips of quartz and calcite that are perpendicular to the vein–host interface. Quartz fibers are the most abundant in the vein (>85% of total number of fibers) and have aspect ratios that vary from 0.5 to 25 with a mean at of 8 (Figs. 6B, 7). Calcite fiber aspect ratios vary from 0.25 to 11 with mean at 4.5. The calcite in fibers is twinned.

Although the quartz fibers show optical continuity along their length, this optical continuity is interrupted in areas where a particular fiber is irregular in shape (Fig. 7B and C). Fiber shapes in lengthwise section can be straight rectangular where fiber width is constant over the length of the fiber or where lensatic fiber width increases along the fiber length toward the center of the fiber (Fig. 7A and B). Fibers contain fluid inclusions arrayed both in bands aligned parallel to the host–vein interface and in trails aligned parallel to the long axis of the fibers. Rock inclusion bands are ubiquitous in quartz fibers whereas rock inclusion trails are exclusive to thick fibers (>100 μm). Thick fibers may show more than one trail spanning an entire fiber length (Fig. 7A through E).

Contacts between fibers are jagged as has been observed by many others (e.g., Ramsay, 1980; Cox and Etheridge, 1983; Cox, 1987; Fisher and Brantley, 1992). The steps along fiber-to-fiber contacts are between 5 and 25 μm or about the same size as veinlet thickness (Figs. 6B and 7B and C). False-color SEM-CL shows growth bands parallel to the vein–host interface that are similar in thickness to that of the veinlets. Growth bands disappear toward the center of fibers. Under false-color SEM-CL, long fibers display ribbons that luminesce in blue parallel to the vein–host interface with shapes and sizes similar to veinlets. These ribbons are commonly enclosed inside the fibers, traversing the fibers from edge-to-edge, but do not

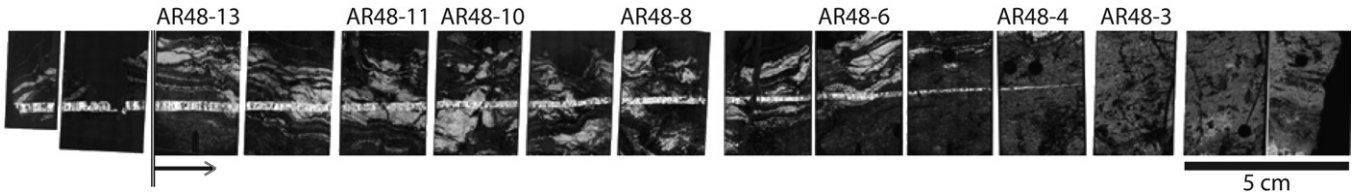

Fig. 5. Crossed-polar photomicrographs of the thin sections comprising vein AR-48.

continue across fiber–fiber contacts. We interpret these features as remnants of original veinlets (Figs. 7D and 9A).

4.4. Host-fiber contacts

Measurements of detrital quartz grains from several thin sections of both fine and coarse-grained host show that the dimensions of the largest grains in the host have dimensions of the same order as the thinnest quartz fibers in the vein (between 20 and 100 μm; Fig. 10). Fiber width in veinlets cutting fine-grained host is thinner than those in veinlets cutting coarse-grained host, less than 20 μm vs. 10 and 50 μm, respectively (Fig. 11D and F).

Host mineralogy influences fiber composition. Calcite fibers in the vein are only found adjacent to calcite-rich laminations in the host.

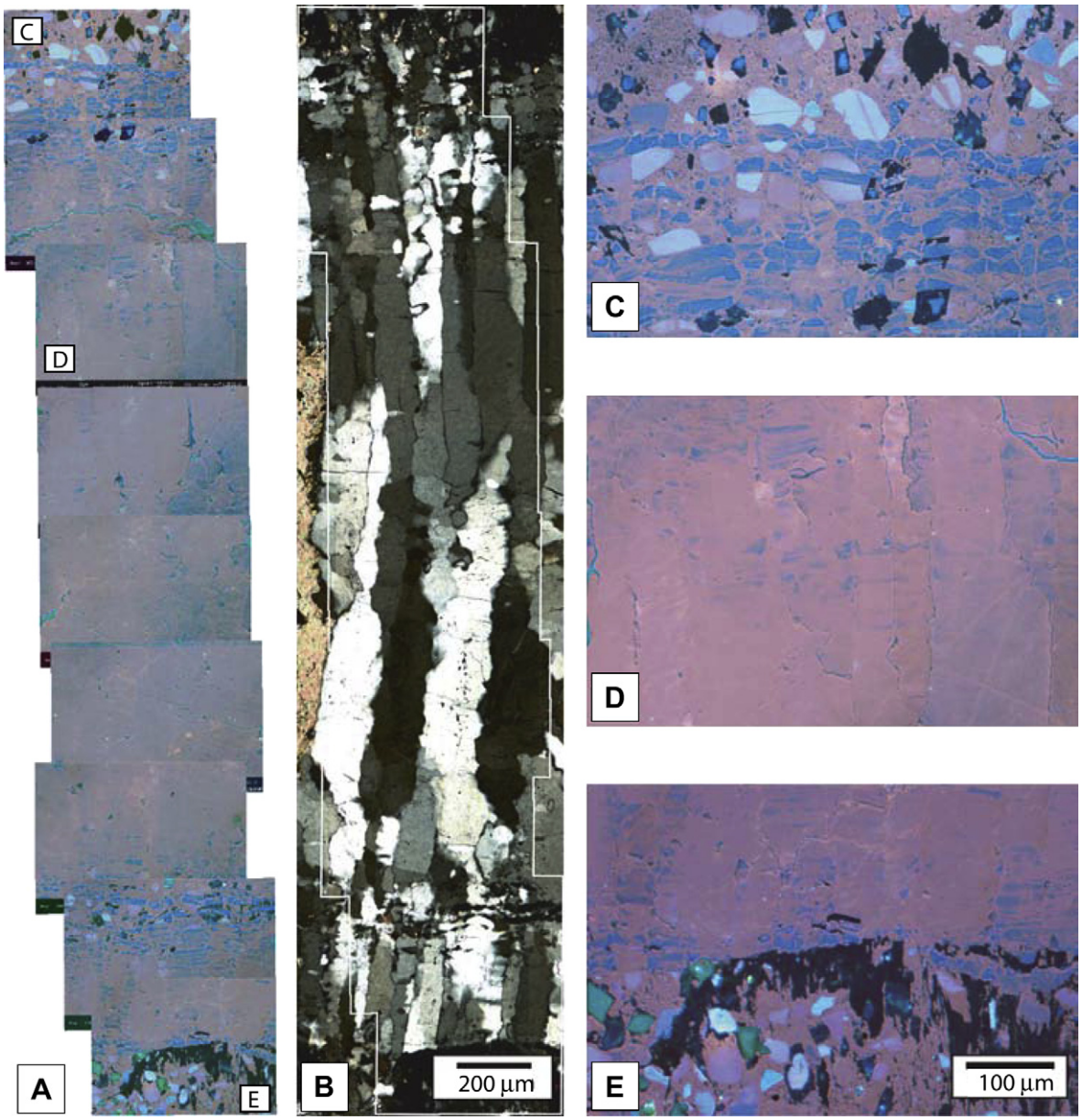

Fig. 6. Polychromatic SEM-CL photomosaic of a section from sample AR-48-13. (A) Polychromatic SEM-CL photomosaic of entire vein width. (B) Optical photomosaic under crossed-polars showing same area of A. (C) SEM-CL photograph from host–vein interface showing fractured host grains. (D) SEM-CL photograph from main body of vein. (E) SEM-CL photograph of host–vein interface showing sliver of host. See location on Fig. 7.

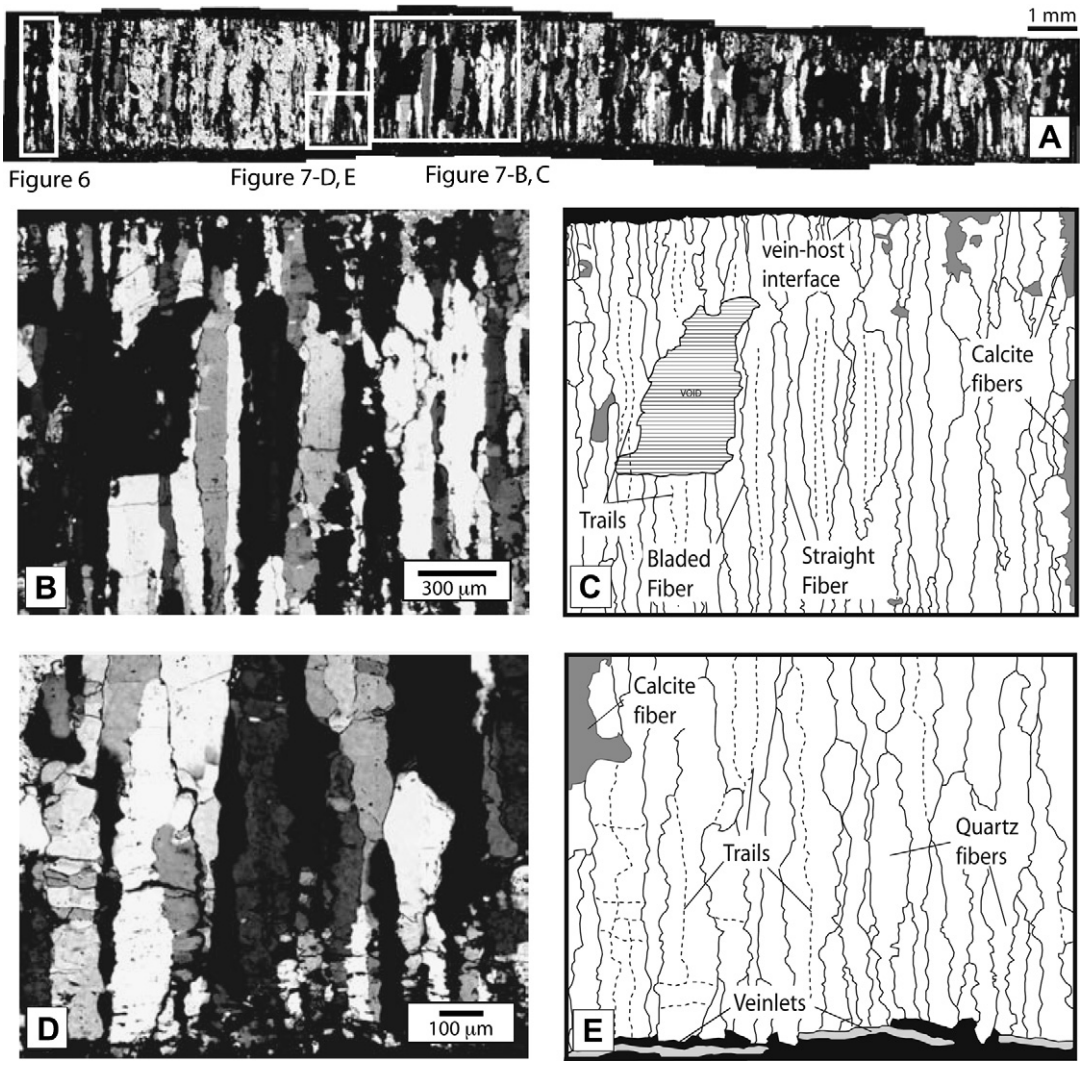

Fig. 7. Photomicrographs showing mid-region vein characteristics. (A) Photomicrograph from section AR-48-13 showing the complete vein. (B) Photomicrograph of a segment from section AR-48-13. (C) Line trace of (B). (D) Close up photomicrograph of a segment from section AR-48-13. (E) Line trace of (D).

The number of veinlets decreases adjacent to coarse-grained host but increases adjacent to fine-grained host (Fig. 11A and B). This observation is consistent throughout the length of the vein.

4.5. Textural comparison between vein center and vein tip

The most distinctive differences between the tip and middle of the vein are: (1) the host–vein interface in the central part of the vein is smooth and well defined (Fig. 7) yet irregular and difficult to define at the tip (Fig. 8). (2) The average fiber width increases from the tip to the center of the vein (Fig. 12). The thinnest fibers in all sections have similar values ranging between 50 and 100 μm (Fig. 12A). The thickest fibers are only found in the center of the vein and they range between 150 and 350 μm (Fig. 12A and B). Wide fibers (>150 μm) show fluid inclusion trails parallel to fiber long axes (Fig. 7). Fibers that span the whole width of the vein are more abundant close to the tip (~80% of the fibers) than at the center of the vein (<15%), although out-of plane fiber trajectories may be a factor in the wider vein center.

Veinlets are less abundant in the center of the vein than in the tip, as they represent between 5% and 20% of the total volume of the vein at the central region (Fig. 7), versus 40 and 100% at the tip (Figs. 8B, D and 13). Host bands parallel to the vein–host interface are more abundant in the tip-region and the proportion of the host inclusions in the vein decreases toward the vein center (Figs. 8, 9 and 13). The number of veinlets decreases toward the tip to the point where the tip consists of only one veinlet (Fig. 13). Under SEM-CL, fibers close to the tip contain more and better defined blue luminescent bands than fibers in the central region of the vein (Figs. 6 and 9A). Host inclusions close to the tip retain the host luminescence whereas fibers at the center of the vein do not show this remnant luminescence (Fig. 6).

5. Discussion

5.1. Vein origin

This vein displays many but not all of the textural features described in the literature as evidence for the crack-seal process. Among these observations are: (1) the same minerals are found in both vein and host (Ramsay, 1980; Cox, 1987; Fisher and Brantley, 1992; Hilgers and Urai, 2002), (2) the fibers in the vein maintain

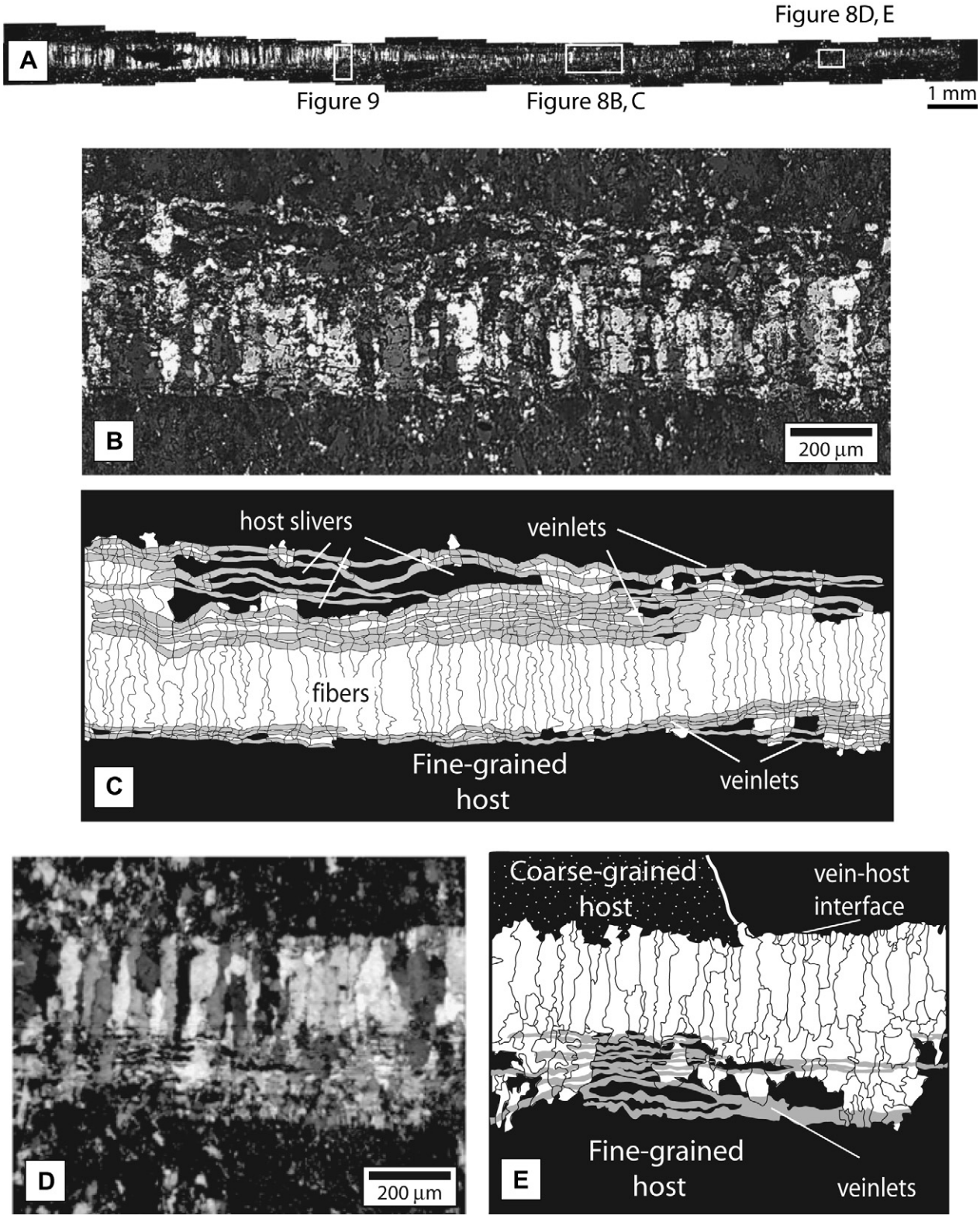

Fig. 8. Photomicrographs showing tip-region vein characteristics. (A) Photomicrograph from section AR-48-4 showing the complete vein. (B) Photomicrograph of a segment from section AR-48-4. (C) Line trace of (B). (D) Close up photomicrograph of a segment from section AR-48-4. (E) Line trace of (D).

the same optical orientation even where the fiber walls change orientation (Ramsay, 1980; Cox and Etheridge, 1983; Fisher and Brantley, 1992; Bons and Jessell, 1997; Bons, 2000; and Hilgers and Urai, 2002), and (3) the fiber width is similar to host grain size (e.g., Cox and Etheridge, 1983). The Ouachita vein also shows regularly spaced fluid-inclusion bands that cross-cut vein fibers parallel to the vein–host interface. These are typically interpreted as sealed fractures (e.g., Laubach, 1988). This vein does not show

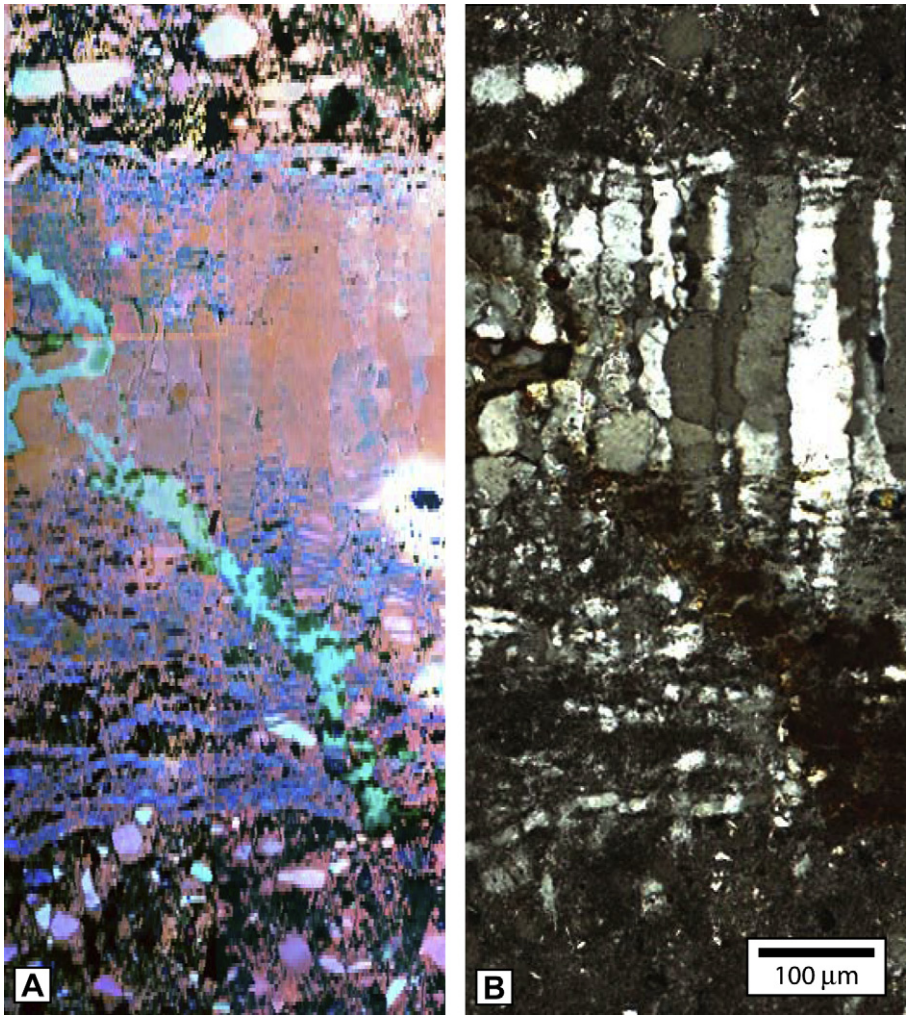

Fig. 9. Polychromatic SEM-CL photomosaic of a section from sample AR-48-4. (A) Polychromatic SEM-CL photomosaic of entire vein width. (B) Optical photomosaic under crossed-polars showing same area of A. See location in Fig. 8.

solid inclusion bands of different mineralogy than the fiber as described in other studies (e.g., Ramsay, 1980; Cox and Etheridge, 1983; and Fisher and Brantley 1992).

Although the vein has several characteristics similar to those described in veins from other studies, it also displays uncommon features. The most striking are the veinlets, which are observed throughout the vein's length. They are described in the literature as: (1) thin filled fractures with no clear localization of the growth surface (Durney and Ramsay, 1973), (2) fracture and precipitation sites responsible for the formation of stretched-crystals (Passchier and Trouw, 1996) and (3) planar vein segments separated by short wall segments, inclined or at moderate angles to the vein margin (Cox, 1987).

Fracturing and precipitation result in the formation of veinlets. Each veinlet represents a distinct filled fracture. We suggest that repeated veinlet formation in largely the same place add up to form the vein. The evidence we have described is that: (1) the tip of the vein is a single veinlet, (2) fractured host grains are cut by veinlets and the host fragments are separated by the veinlet mineralization, (3) toward the center of the vein they are always present at the edge between vein and host, (4) veinlets become less distinct toward the center of the vein, and (5) fibers show growth bands with similar luminescence signature as veinlets parallel to host–vein interface. These growth bands represent remnants of fracturing events.

The decreasing proportion of host grains toward the center of the vein might hold a further clue to vein origin. As discussed previously, the veinlet–host proportion is <1 at the vein tip. Host inclusions in the first observed fibers in going from the vein tip to center are common at first but then decreasingly so toward the vein center. Host inclusions in, for example, Fig. 9, are only observed toward or at the vein margin. There are at least three possibilities for the decreasing proportion of host inclusions from tip to center: (1) the host inclusions are dissolved, phyllosilicates and all; (2) the host inclusions are confined to the tip because subsequent veinlets preferentially form at veinlet boundaries so that after a certain disorganized start, no more host is included in the vein; and/or (3) host is present but the proportion is both very small and perhaps altered by recrystallization. We prefer a combination of (2) and (3), noting that host inclusions are everywhere more prevalent on the vein–host wall and adjacent to more phyllosilicates-rich fractions of the host. Repeated fracturing, in this interpretation took place within the vein.

5.2. Fiber growth and modification

Textures suggest that fibers are modified subsequent to formation. The observations leading to this suggestion are: (1) increasing fiber width with distance from the vein tip; (2) presence of inclusion trails inside wide fibers (>100 µm) parallel to the long axis of

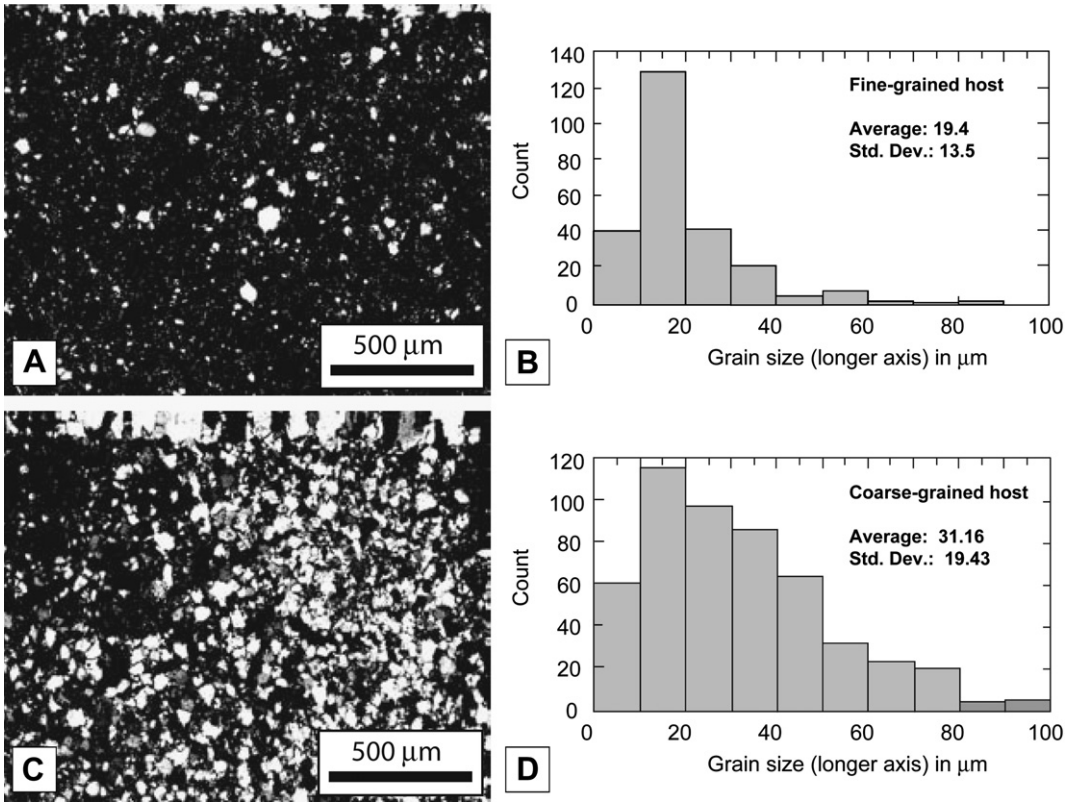

Fig. 10. Comparison between coarse-grained and fine-grained hosts. (A) Photomicrograph of a fine-grained section (sample AR-48). (B) Histogram of grain size distribution for fine-grained host. (C) Photomicrograph of coarse-grained host section (sample AR-48). (D) Histogram of grain size distribution for coarse-grained host.

the fiber; we interpret these as previous fiber–fiber contacts that were incorporated in a wider fiber; (3) fiber widths are larger toward the center of the vein although thin fibers (on the order of host grain sizes) are observed throughout the vein length; (4) the spacing of inclusion trails in thick fibers is similar to the widths of thin fibers without inclusion trails and, (5) the difference in luminescence between the quartz in the veinlets and the quartz in the fibers along the main body of the vein. Remnants of veinlets are displayed in fibers as blue CL stripes parallel to the vein–host interface. If there had been no change in the fiber quartz, then presumably the CL color throughout the fibers would be the same as that in the veinlets.

5.2.1. Fiber width

The observation suggests that fibers grow laterally at the expense of previously formed fibers suggests that one or both of the following have taken place: (1) preferential dissolution of particular quartz faces and/or (2) differential dissolution of different quartz faces due to differences in rate of growth. Preferential dissolution of particular quartz faces can be tied to the composition of impurities preferentially incorporated along particular crystallographic orientations (Ihinger and Zink, 2000). For example, AlOH defects can be preferentially oriented along channels that run parallel to the *c*-axis. Dove (1999) and Dove et al. (2005) showed that quartz dissolution rates are inhibited by the presence of Al and Fe. These two observations combined would result in the preferential dissolution of quartz faces with less Al impurities. The second process suggests that preferential dissolution of quartz faces can be tied to differences in rate of growth for different crystal faces. Iwasaki et al. (1998) evaluated growth rates for different quartz faces comparing synthetic quartz growth experiments against computer generated geometrical crystal growth experiments. They observed that the rate of crystal growth parallel to *c*-axis is 5 times faster than the next fastest crystal face (r-face) and more than 150 times faster than the slowest crystal face (m-face). The same effect of growth rate with orientation was described by Lander et al. (2002) and Laubach et al. (2004b) in natural quartz veins under cathodoluminescence. These studies suggest that dissolution–reprecipitation processes will favor crystallographic orientations with faster growth rates. Either of these or a combination of the processes could be the driving force for grain- boundary migration where dissolution of less stable quartz orientations (e.g., faces with less Al impurities and/or faces growing at slower rates) and further precipitation of more stable ones occurs along fiber–fiber contacts.

5.2.2. Fiber luminescence

Although cited above as evidence of fiber modification, the significance of the luminescence difference between fibers and veinlets is difficult to establish with certainty. Differences in luminescence represent variations in the chemistry and concentration of the impurities in the quartz (Hervig and Peacock, 1989; Perny et al., 1992; Watt et al., 1997; Monecke et al., 2002). Goldstein and Rossi (2002) propose that the differences in luminescence may be due to the presence of precursor phases such as opal-CT, cryptocrystalline quartz or microcrystalline quartz. They observed that overgrowths on detrital sand grains under SEM-CL followed the crystallographic orientations of the detrital grains and suggested that the observed textures of growth banding and growth zoning could be explained as recrystallization of bands of an unstable form of silica. This conclusion was disputed by Lander et al. (2008) who experimentally produced similar textures without observing a precursor phase.

The presence of impurities in quartz has also been shown to be related to crystal growth rates. Ihinger and Zink (2000) analyzed

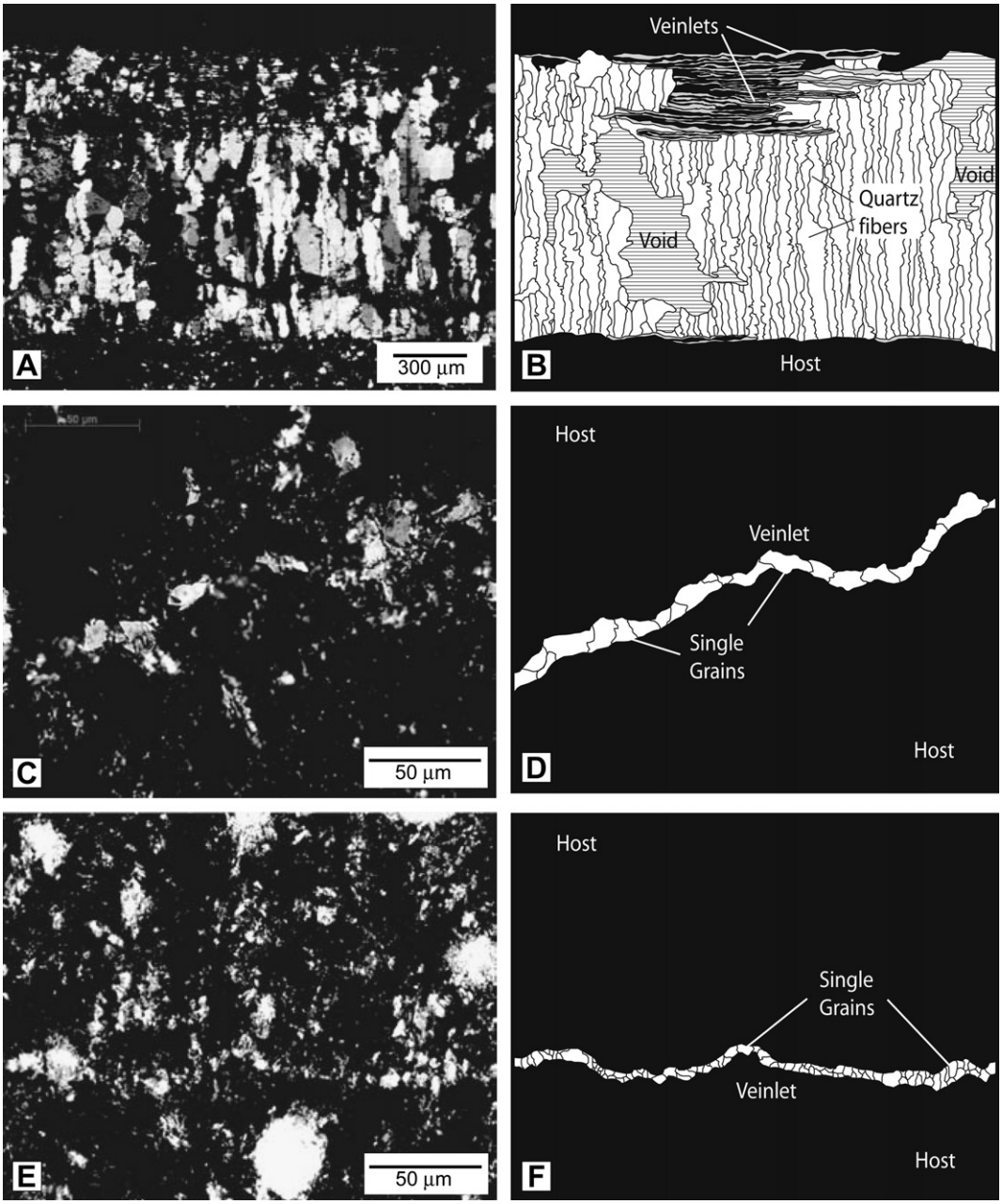

Fig. 11. Photomicrographs showing veinlet characteristics. (A) Photomicrograph from section AR-48-6 showing the irregular distribution of veinlets along a vein section. Veinlets start and/or end at fibers. Veinlet width is constant along their length. (B) Line trace of (A). (C) Photomicrograph of one veinlet cutting across coarse-grained host at section AR-48-13. (D) Line trace of (C) showing the important features. (E) Photomicrograph of one veinlet cutting across fine-grained host. (F) Line trace of (E).

the geochemical variations as well as concentration of impurities of three different hydrous species (AlOH, LiOH and HOH) through different cuts across a single Brazilian crystal. Where embedded within the crystal, these impurities provide a continuous record of the relative growth rate of the individual crystal faces. Watson and Liang (1995) and Paquette and Reeder (1995) showed that impurity concentrations will increase with increasing growth rate independent of pressure and temperature of the environment. Ihinger and Zink (2000) in turn proposed that for a crystal that grows at a rate too fast to maintain equilibrium, impurity concentrations will increase with increasing growth rate, producing chemically distinguishable zones. See also Kawasaki (2003).

We suggest that the differences in luminescence between the quartz precipitated in the veinlets and the quartz fibers can be explained by two processes involving different rates, similar to the observations of Ihinger and Zink (2000). For example, if the rate of precipitation of the veinlet quartz was fast because the fluid was far from equilibrium (i.e., highly supersaturated), the precipitating quartz would contain high impurity concentrations. If instead the quartz precipitated at a slower rate from a fluid closer to equilibrium after recrystallization, the quartz would contain fewer impurities.

5.2.3. Timing of calcite vs. quartz fibers

The origin and timing of the vein calcite is not certain, and this uncertainty may be a confounding factor in interpreting along-axis fiber width changes as due to recrystallization. Laubach (2003) and Laubach et al. (2004a, b) observed post-kinematic vein fills in rocks that were buried less deeply our vein. They observed calcite

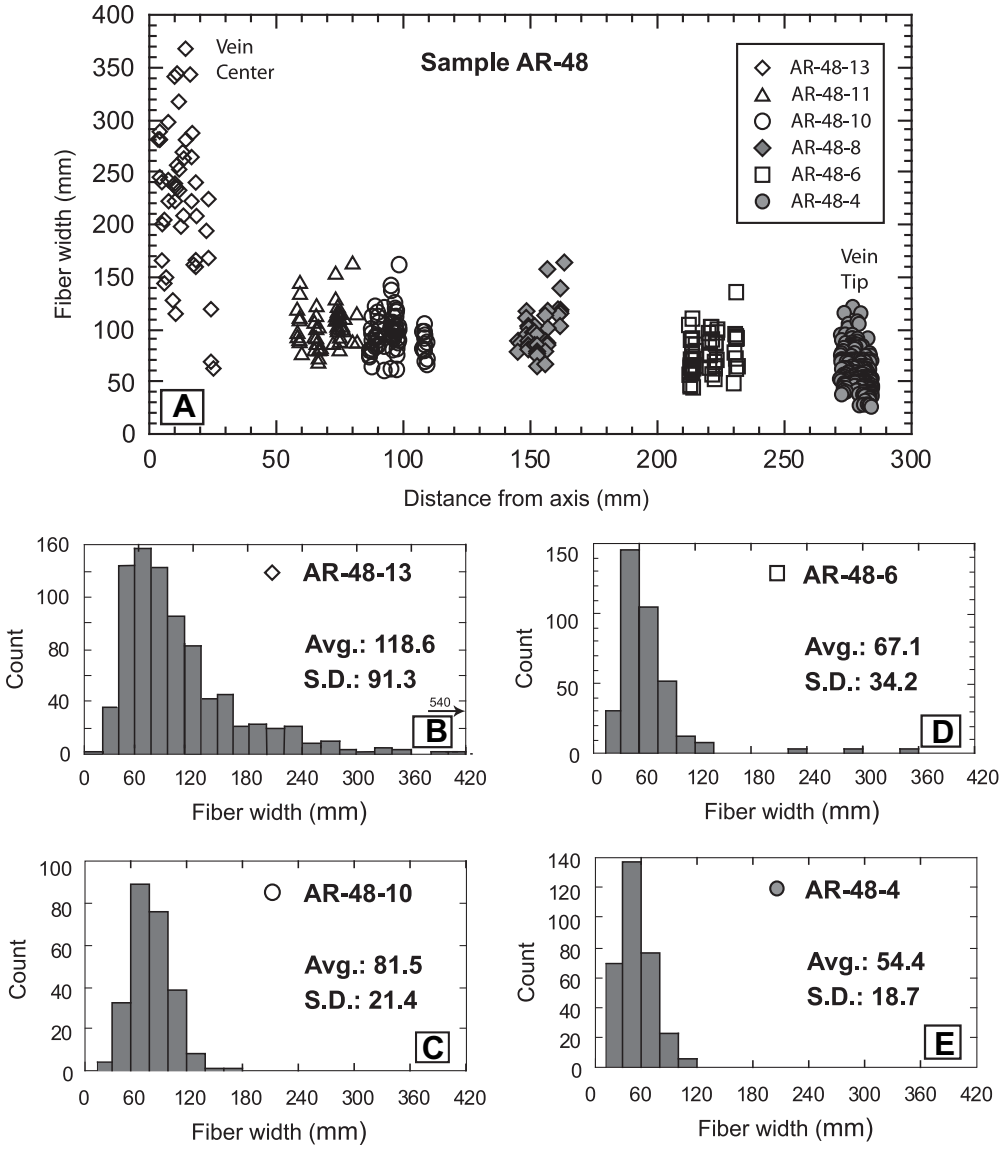

Fig. 12. Plot of fiber width vs. distance from midpoint (*x*-axis on Fig. 5) for sample AR-48. For the plot only fibers spanning the entire width of the vein were considered. (A) Plot of measurements from sample AR-48 (thin sections 4, 6, 8, 10, 11, and 13). (B) Histogram of fiber widths from sample AR-48-13. (C) Histogram of fiber widths from sample AR-48-10. (D) Histogram of fiber widths from sample AR-48-6. (E) Histogram of fiber widths from sample AR-48-4.

commonly surrounding quartz bridges across partially open fractures. The quartz bridges may display terminated crystals on their sides which, presumably, grew into open space before the calcite was precipitated over them. While the bridge may show "crack-seal" texture, the calcite does not, suggesting that the calcite did not participate in the repeated fracture episodes leading to fracture aperture (Laubach, 1988). Laubach and Ward (2006) further observed thin layers of unfractured, zoned quartz that overlaps crack-seal texture along bridge edges, showing the precipitation continued after fracturing.

Our observations on the fibers toward the center of the vein do not argue for appreciable porosity at any stage of this vein's growth. Although the small amount of calcite might be late, especially the blocky grains, most calcite fibers are surrounded by other quartz fibers. We observe no quartz terminations along the side of the fibers as the only observed quartz terminations are at the tip of this vein tip in veinlets. There is no coating of uniformly luminescent quartz on fiber boundaries; the fiber-normal laminations that we have interpreted as remnant veinlets extend from edge-to-edge of the fibers. Therefore, from the observation of vein texture we suggest that vein evolution and growth involves: (a) fracturing and precipitation and (b) later recrystallization perhaps accompanied by dissolution and precipitation along fiber boundaries.

5.3. Association of veins and boudinage

Our field observations show that veining and boudinage are closely associated. We suggest that boudinage is responsible for the localization of the stress required to form these veins.

The means by which fracturing is localized has been one of the concerns of previous authors. Ramsay (1980) and Cox and Etheridge (1983) suggest that fracturing occurred along areas of strength contrast in the host enhanced by abnormal fluid pressure. Fisher and Brantley (1992) and Fisher et al. (1995) suggest that fracturing occurs at the host vein interface due to lower cohesion between the host rock and the newly precipitated

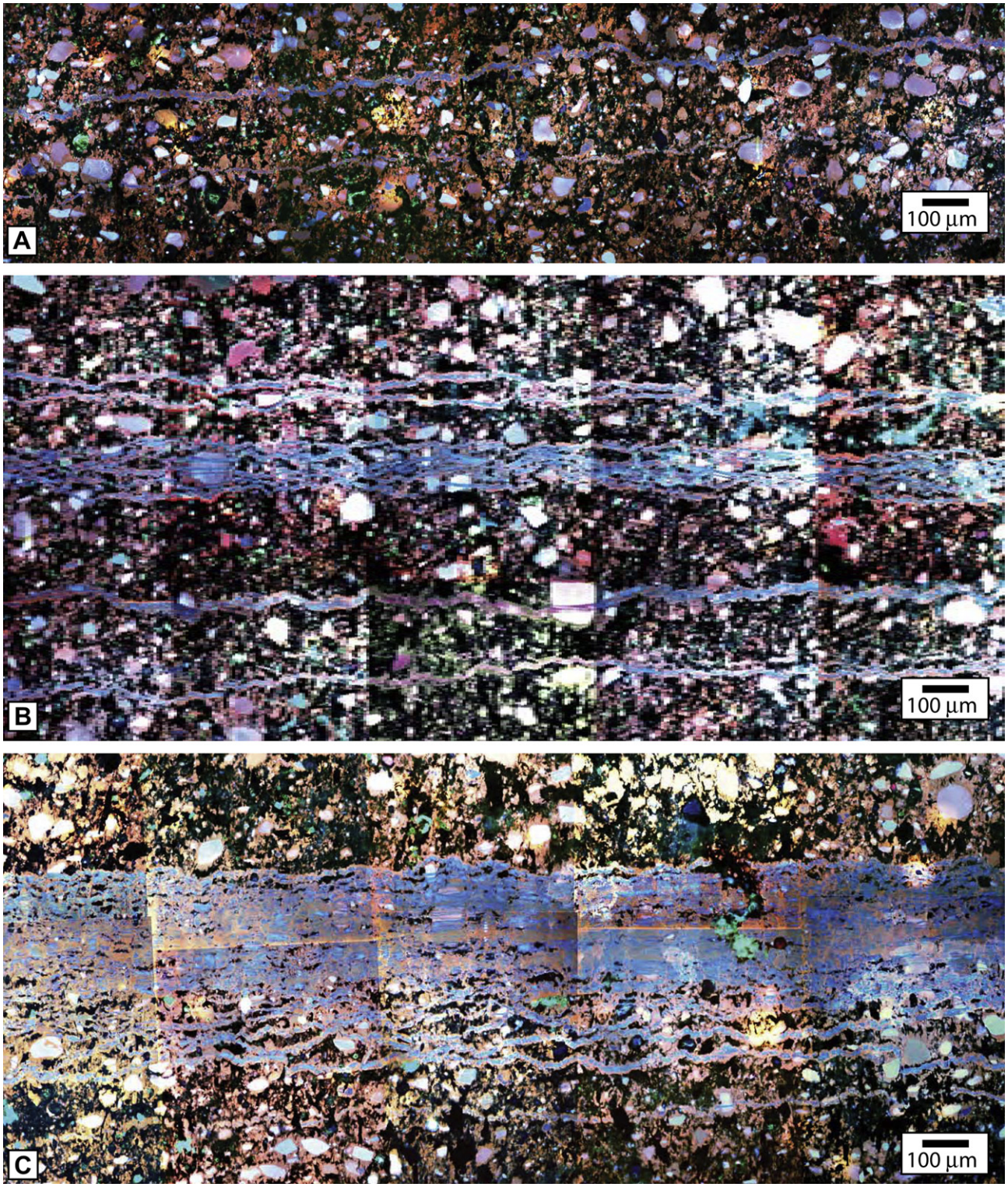

Fig. 13. Veinlet textures as the vein tip is approached. Polychromatic SEM-CL photomosaic of one segment of section AR-48-4 and two segments of section AR-48-3. (A) Polychromatic SEM-CL photomosaic of the segment from section AR-48-3 closest to the tip. (B) Polychromatic SEM-CL photomosaic of the segment from section AR-48-3 adjacent to section AR-48-4. (C) Polychromatic SEM-CL photomosaic of the segment from section AR-48-4 adjacent to section AR-48-3.

material. Taber (1916, 1920), Means and Li (2001) and Wiltschko and Morse (2001) suggest that fracture propagation and subsequent vein widening is caused by pressure due to growing crystals.

In the Lake Pineda outcrop, boudinage is observed at several scales. Large veins (meters long and 10′s of cm wide) are associated with boudinage necks formed in sandstone layers 10′s of centimeters thick whereas thin and elongated veins (cm long and up to 1 cm wide) are found in thin (<1 cm) sandstone beds. The vein width is a function of the thickness of the host sandstone layer. The close relationship between boudins and veins has been described

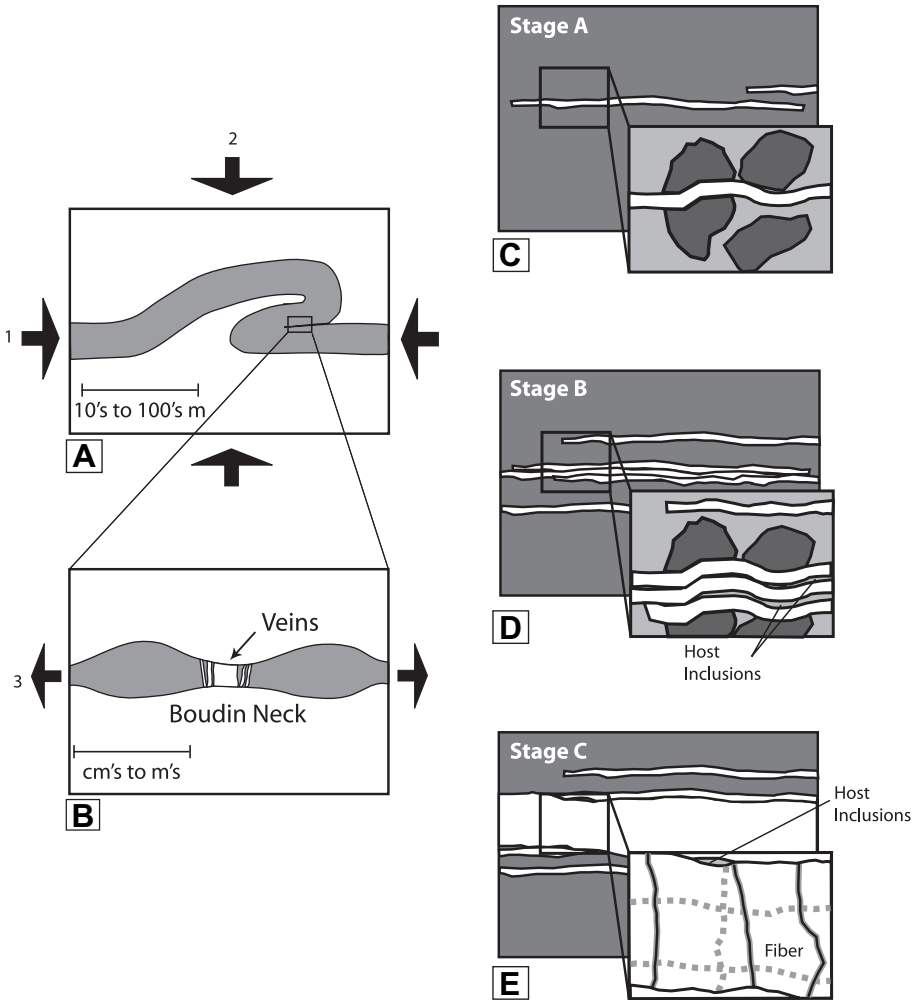

Fig. 14. Schematic diagram showing vein growth model. See explanation of stages in text. (A) and (B) tectonic events leading to the formation of boudins. (C)–(E) Stages A–C of vein formation.

by many authors (e.g., De Paor et al., 1991; Swanson, 1992; Sintubin et al., 2000; Bojar et al., 2001; Urai et al., 2001).

Several mechanical models are proposed for boudin formation (e.g., Smith, 1977; Mandal et al., 2000; Pollard and Fletcher, 2005; Passchier and Druguet, 2002). All models attribute the formation of boudinage to the viscosity contrast between the layer containing the boudins and the material surrounding it as the layer is loaded normal to layering. The distance between boudin necks is a function of both layer thickness and viscosity contrast between layers. Pollard and Fletcher (2005) considered boudinage in an isotropic power-law fluid embedded in a plastic solid. Their model shows that stress perturbations or deviations from the mean stress are negative where the layer is thinnest. Ignoring gravity, these negative perturbations correspond to tensile stresses in the layer. This model shows that once pinching of the stronger layer starts, stresses localized at these thin regions of the boudin necks.

Boudinage in the Lake Pineda outcrop always occurs when a layer of sandstone is surrounded by slate. The differences in mechanical properties of these rocks allowed the localization of stresses at the boudin necks, leading to dilation and subsequent vein formation. Modeling results indicate that the repeated, highly localized, cracking required to form our vein is controlled by boudinage of the sandstones.

6. Integrated kinematic-chemical model

Consideration of vein formation begins at the tectonic scale where the emplacement of large duplexes at depth (Nelson, 1982; Viele, 1989) perturbed the stress field in the host rocks from the veins such that the maximum principal stress became vertical rather than horizontal. This rotation caused the flattening of the host sedimentary sequence (Fig. 14B). Flattening of the overturned and fractured fold limbs triggered dissolution giving rise to cleavage and layer-parallel extension of the more resistant layers, resulting in the formation of boudinage of the sandstone layers creating the circumstances for vein formation (Fig. 14C).

The local stages involved in vein formation follow the evolution of the encasing boudin. Stage A: Individual fractures originated at the necks of boudins. Fracturing along necks generated chemical potential gradients allowing vein forming material to diffuse toward the neck and precipitate. Coarse-grained host layers and cleavage planes acted as paths for the vein forming material. As layer parallel-extension continued, fracturing events where localized along the necks in areas where strength contrast between newly precipitated material and host rock where greatest (Fig. 14D). Host slivers are predominantly separate different veinlets at this stage. Stage B: Host grains acted as seeds for fibers. Progressive fracturing events cut across grains in the host, particularly along coarse-grained host. This

process generated clean surfaces where a supersaturated fluid precipitated quartz using the host grain as template for growth, maintaining its crystallographic orientation. Repetition of this process allowed fibers to grow (Fig. 14E). As fracturing becomes localized, the volume of host inclusions to vein material is reduced. Stage C: Recrystallization of early precipitated quartz into stable crystallographic orientation of the fibers. This process changed the composition of the newly precipitated quartz as evidenced by differences in luminescence colors. This process caused vein fibers to grow laterally in width (Fig. 14F).

7. Conclusions

Examination of a vein from its tip to center, shows the transition from a single filled fracture at the vein tip to typical "crack-seal" textures observed fibered, laminated veins. The two fabric elements of this vein are veinlets and fibers. Veinlets are defined as quartz-filled narrow (5–25 μm) veins parallel or at low angle to the host–vein interface. The tip of the vein is composed of one or a small group of them. Scanned SEM-CL shows that quartz laminae of the same orientation, thickness and luminescence are found throughout the vein. Assuming that the vein geometry at the tip represents early vein geometry at the vein center, wall-normal fibers appear early in going from the tip toward the vein center. They first appear in the vein where detrital grains are cut by multiple veinlets with each of the veinlets mimicking the crystallographic orientation of the detrital grain. By contrast, later veinlets reflect the established crystallographic orientation of the fiber. At the vein center, the body of the vein is predominantly formed by fibers whereas the tip region is formed by veinlets. Fibers throughout the vein retain evidence of formation by repeated fracturing and filling of a pre-existing grain (at the vein walls) or fiber. Recrystallization later modified the fibers by obliterating some evidence of the veinlets. Some fibers in the vein center also widen at the expense of adjacent ones. The stress localization required for the formation and growth of these veins is controlled by local structures. Boudinage formation provided the extension site in the boudin neck that localized fracturing and vein filling. The vein grows by both length and width by the repeated addition of veinlets in the boudin neck region.

Acknowledgements

Grants from AAPG, GSA to PC and The Texas Advanced Research Program and NSF award EAR-0107079 to DVW supported this project. The FE-SEM acquisition was supported in part by the National Science Foundation under Grant No. DBI-0116835. We would like to thank Ray Guillemette of the Department of Geology and Geophysics Electronic Microprobe Lab and Tom Stephens of the TAMU Microscopy and Imaging Center for their help acquiring element maps and SEM-CL images, respectively. We thank Steve Laubach and Chris Hilgers for providing thoughtful reviews that measurably improved the manuscript. We finally thank editor Bill Dunne for his stewardship of this manuscript.

References

Arbenz, J.K.. 1989. The Ouachita system. In: Bally, A.W. and Palmer, A.R. (Eds.), The Geology of North America – an Overview A, Geological Society of North America, Bolder, Colorado, 371–396.

Arne, D.C., 1992. Evidence from apatite fission-track analysis from regional Cretaceous cooling in the Ouachita mountain fold belt and Arkoma basin of Arkansas. American Association of Petroleum Geologist Bulletin 76, 392–402.

Bass, M.N., Ferrara, G., 1969. Age of adularia and metamorphism, Ouachita mountains, Arkansas. American Journal of Science 267, 491–498.

Bignall, G., Sekine, K., Tsuchiya, N., 2004. Fluid-rock interaction processes in the Te Kopia geothermal field (New Zealand) revealed by SEM-CL imaging. Geothermics 33, 615–635.

Bojar, H.P., Bojar, A.V., Mogessie, A., Fritz, H., Thalhammer, O.A.R., 2001. Evolution of veins and sub-economic ore at Strassegg, Paleozoic of Graz, Eastern Alps, Austria: evidence for local fluid transport during metamorphism. Chemical Geology 175, 757–777.

Bons, P.D., Jessell, M.W., 1997. Experimental simulation of the formation of fibrous veins by localized dissolution-precipitation creep. Mineralogical Magazine 61, 53–63.

Bons, P.D., 2000. The formation of veins and their microstructures. Journal of the Virtual Explorer 2, 12.

Cervantes, P., 2007. Tectonic fibrous veins: initiation and evolution, Ouachita orogen, Arkansas, PhD dissertation, Texas A&M University, College Station, TX, p. 120.

Corrigan, J., Cervany, P.F., Donelick, R., Bergman, S.C., 1998. Postorogenic denudation along the late Paleozoic Ouachita trend, south central United States of America: magnitude and timing constraints from apatite fission track data. Tectonics 17, 587–603.

Cox, S.F., Etheridge, M.A., 1983. Crack-seal fibre growth mechanisms and their significance in the development of oriented layer silicate microstructures. Tectonophysics 92, 147–170.

Cox, R., Van Arsdale, R., 1997. Hotspot origin of the Mississippi embayment and its possible impact on contemporary seismicity. Engineering Geology 46, 201–216.

Cox, R., Van Arsdale, R., 2002. The Mississippi Embayment, North America: a first order continental structure generated by the Cretaceous superplume mantle event. Journal of Geodynamics 34, 163–176.

Cox, S.F., 1987. Antitaxial crack-seal vein microstructures and their relationship with displacement paths. Journal of Structural Geology 9, 779–787.

De Paor, D.G., Simpson, C., Bailey, C.M., McCaffrey, K.J.W., Beam, E., Gower, R.J.W., Aziz, G., 1991. The role of solution in the formation of boudinage and transverse veins in carbonate rocks at Rheems, Pennsylvania. Geological Society of America Bulletin 103, 1552–1563.

Denison, R.E., Burke, W.H., Otto, J.B., Hetherington, E.A., 1977. Age of igneous and metamorphic activity affecting the Ouachita foldbelt. In: Stone, C.G. (Ed.), Symposium on the geology of the Ouachita Mountains 1: Arkansas Geological Commission, 26–40.

Dove, P., Han, N., De Yoreo, J.J., 2005. Mechanisms of classical crystal growth theory explain quartz and silicate dissolution behavior. Proceedings of the National Academy of Sciences 102, 15357–15362.

Dove, P., 1999. The dissolution kinetics of quartz in aqueous mixed cation solutions. Geochimica et Cosmochimica Acta 63, 3715–3727.

Durney, D.W., Ramsay, J.G., 1973. Incremental strains measured by syntectonic crystal growths. In: De Jong, K.A., Scholten, R. (Eds.), Gravity and Tectonics. Wiley, New York, pp. 67–96.

Fisher, D.M., Brantley, S., 1992. Models of quartz overgrowth and vein formation: deformation and episodic fluid flow in an ancient subduction zone. Journal of Geophysical Research 97, 20043–20061.

Fisher, D.M., Brantley, S.L., Everett, M., Dzvonik, J., 1995. Cyclic fluid flow through a regionally extensive fracture network within the Kodiak accretionary prism. Journal of Geophysical Research 100, 12881–12894.

Goldstein, R.H., Rossi, C., 2002. Recrystallization in quartz overgrowths. Journal of Sedimentary Research 72 (3), 432–440.

Goscombe, B.D., Passchier, C.W., Hand, M., 2004. Boudinage classification: end-member boudin types and modified boudin structures. Journal of Structural Geology 26, 739–763.

Gotze, J., Plotze, M., Habermann, D., 2001. Origin, spectral characteristics and practical applications of the cathodoluminescence (CL) of quartz – a review. Mineralogy and Petrology 71, 225–250.

Haley, B.R., Stone, C.G., 1996. CoGeo Maps of Arkansas. Arkansas Geological Commission, Little Rock, Arkansas.

Hervig, R.L., Peacock, S.M., 1989. Implications of trace element zoning in deformed quartz from the Santa Catalina mylonite zone. Journal of Geology 89, 343–350.

Hilgers, C., Urai, J.L., 2002. Microstructural observations of natural syntectonic fibrous veins: implications for the growth process. Tectonophysics 352, 257–264.

Houseknecht, D.W., Matthews, S.M., 1985. Thermal maturity of Carboniferous strata, Ouachita Mountains. American Association of Petroleum Geologist Bulletin 69, 335–345.

Ihinger, P.D., Zink, S.I., 2000. Determination of relative growth rates of natural quartz crystals. Nature 404, 865–869.

Iwasaki, H., Iwasaki, F., Balitsky, V.S., Balitskaya, L.V., Makhina, I.B., 1998. Growth rates anisotropy of synthetic quartz crystals grown on Z-cut hexagonal seeds and computer simulations of growth processes. Journal of Crystal Growth 187, 481–489.

Kawasaki, M., 2003. Growth-induced inhomogeneities in synthetic quartz crystals revealed by the cathodoluminescence method. Journal of Crystal Growth 247, 185–191.

Lander, R.H., Gale, J.F.W., Laubach, S.E., Bonnell, L.M., 2002. Interaction between quartz cementation and fracturing in sandstone. American Association of Petroleum Geologists Annual Convention Program 11, A98–A99.

Lander, R.H., Larese, R.E., Bonnell, L.M., 2008. Toward more accurate quartz cement models: the importance of euhedral versus noneuhedral growth rates. American Association of Petroleum Geologists Bulletin 92, 1537–1563.

Laubach, S.E., Lander, R.H., Bonnell, L.M., Olson, J.E., Reed, R.M., 2004a. Opening histories of fractures in sandstone. In: Cosgrove, J.W., Engelder, T. (Eds.), The

initiation, propagation and arrest of joints and other fractures, Geological Society London Special Publications, 231, pp. 1–9.
Laubach, S.E., Reed, R.M., Olson, J.E., Lander, R.H., Bonnell, L.M., 2004b. Coevolution of crack-seal texture and fracture porosity in sedimentary rocks: cathodoluminescence observations of regional fractures. Journal of Structural Geology 26, 967–982.
Laubach, S.E., Ward, M.E., 2006. Diagenesis in porosity evolution of opening-mode fractures, Middle Triassic to Lower Jurassic La Boca Formation, NE Mexico. Tectonophysics 419, 75–97.
Laubach, S.E., 1988. Subsurface fractures and their relationship to stress history in East Texas Basin sandstone. Tectonophysics 156, 37–49.
Laubach, S.E., 2003. Practical approaches to identifying sealed and open fractures. American Association of Petroleum Geologist Bulletin 87, 561–579.
Li, T., 2000. Experimental Growth of Fibers and Fibrous Veins, Unpublished Doctor of Philosophy Thesis, University at Albany, State University of New York.
Lillie, R.J., Nelson, K.D., de Voogd, B., Brewer, J.A., Oliver, J.E., Brown, L.D., Kaufman, S., Viele, G.W., 1983. Crustal structure of Ouachita Mountains, Arkansas: a model based on integration of COCORP reflection profiles and regional geophysical data. American Association of Petroleum Geologist Bulletin 67, 907–931.
Lowe, D.R., 1989. Stratigraphy, sedimentology, and depositional setting of preorogenic rocks of the Ouachita Mountains, Arkansas and Oklahoma. In: Hatcher, R.D., Thomas, W.A., Viele, G.W. (Eds.), The Appalachian-Ouachita Orogen in the United States. Geological Society of America. DNAG, The Geology of North America F-2, Boulder, Colorado, pp. 575–590.
Mandal, N., Chakraborty, C., Kumar Samanta, S., 2000. Boudinage in multilayered rocks under layer-normal compression: a theoretical analysis. Journal of Structural Geology 22, 373–382.
Means, W.D., Li, T., 2001. A laboratory simulation of fibrous veins: some first observations. Journal of Structural Geology 23, 857–863.
Milliken, K.L., Laubach, S.E., 2000. Brittle Deformation in Sandstone Diagenesis as Revealed by Scanned Cathodoluminescence Imaging with Application to Characterization of Fractured Reservoirs. In: Cathodoluminescence in Geosciences. Springer Verlag, New York, pp. 225–243(Chapter 9).
Miser, H.D., 1959. Structure and vein quartz of the Ouachita Mountains of Arkansas and Oklahoma. In: Cline, L.M., Hilsewick, W.J., Feray, D.E. (Eds.), Ouachita Symposium. Dallas and Ardmore Geological Societies, Dallas, Texas, pp. 30–43.
Misik, M., 1971. Observations concerning calcite veinlets in carbonate rocks. Journal of Sedimentary Petrology 41, 450–460.
Monecke, T., Kempe, U., Götze, J., 2002. Genetic significance of the trace element content in metamorphic and hydrothermal quartz: a reconnaissance study. Earth and Planetary Science Letters 202, 709–724.
Nelson, K.D., Lillie, R.J., de Voogd, B., Brewer, J.A., Oliver, J.E., Kaufman, S., Brown, L.D., Viele, G.W., 1982. COCORP seismic reflection profiling in the Ouachita Mountains of western Arkansas: Geometry and geologic interpretation. Tectonics 1, 413–430.
Nielsen, K.C., Viele, G.W., Zimmerman, J,, 1989. Structural setting of the Benton-Broken Bow uplifts. In: Hatcher, R.D., Thomas, W.A., Viele, G.W. (Eds.), The Appalachian-Ouachita Orogen in the United States. DNAG, The Geology of North America F-2. Geological Society of America, Boulder, Colorado, pp. 575–590.
Pagel, M., Barbin, V., Blanc, P., Ohnenstetter, D. (Eds.), 2000. Cathodoluminescence in Geosciences. Springer-Verlag, New York.
Paquette, J., Reeder, R., 1995. Relationship between surface structure, growth mechanism, and trace element incorporation in calcite. Geochimica et Cosmochimica Acta 59, 735–749.
Passchier, C.W., Druguet, E., 2002. Numerical modelling of asymmetric boudinage. Journal of Structural Geology 24, 1789–1803.
Passchier, C.W., Trouw, R.A.J., 1996. Microtectonics. Springer, Berlin.
Perny, B., Eberhardt, P., Ramseyer, K., Mullis, J., Pankrath, R., 1992. Microdistribution of aluminum, lithium, and sodium in a quartz: possible causes and correlation with short lived cathodoluminescence. American Mineralogist 77, 791–800.
Pollard, D.D., Fletcher, R.C., 2005. Fundamentals of Structural Geology. Cambridge University Press, Cambridge, 500 pp.
Ramsay, J.G., 1980. The crack-seal mechanism of rock deformation. Nature 284, 135–139.
Reed, R.M., Milliken, K.L., 2003. How to overcome imaging problems associated with carbonate minerals on SEM-based cathodoluminescence system. Journal of Sedimentary Research 73, 328–332.
Shelton, K.L., Reader, J.M., Ross, L.M., Viele, G.W., Seidemann, D.E., 1986. BA-rich adularia from the Ouachita Mountains, Arkansas: implications for a post-collision hydrothermal system. American Mineralogist 71, 916–923.
Sintubin, M., Kenis, I., Schroyen, K., Muchez, P., Burke, E.A.J., 2000. "Boudinage" in the High-Ardenne slate belt (Belgium), reconsidered from the perspective of the "interboudin" veins. Journal of Geochemical Exploration 69–70, 511–516.
Smith, R.B., 1977. Formation of folds, boudinage, and mullions in non-Newtonian materials. Geological Society of America Bulletin 88, 312–320.
Stone, C.G., McFarland, J.D., 1981. Field guide to the Paleozoic rocks of the Ouachita Mountain and Arkansas Valley Provinces, Arkansas. In: Arkansas Geological Commission Guidebook. Arkansas Geological Commission Guidebook, Little Rock, Arkansas, pp. 140.
Stone, C.G., Boyd, R.H., Davis, M.H., 1994. Guidebook to Paleozoic Rocks in the Eastern Ouachita Mountains Arkansas. In: Williams, N.F. (Ed.), State of Arkansas. Arkansas Geological Commission, Little Rock, Arkansas, pp. 1–46.
Swanson, M.T., 1992. Late Acadian-Alleghenian transpressional deformation: evidence from asymmetric boudinage in the Casco Bay area, coastal Maine. Journal of Structural Geology 14, 323–341.
Taber, S., 1916. The growth of crystals under external pressure. American Journal of Science 41, 532–556.
Taber, S., 1918. The genesis of asbestos and asbestiform minerals. American Institute of Mining Engineers Transactions 57, 62–98.
Taber, S., 1920. The mechanics of vein formation (with discussion). American Institute of Mining and Metallurgical Engineers Transactions 61, 3–41.
Underwood, M.B., Fulton, D.A., McDonald, K.W., 1988. Thrust control on thermal maturity of the frontal Ouachita Mountains, central Arkansas, USA. Journal of Petroleum Geology 11, 325–339.
Urai, J.L., Spaeth, G., Van der Zee, W., Hilgers, C., 2001. Evolution of Mullion (Boudin) structures in the Variscan of the Ardennes and Eifel. Journal of the Virtual Explorer 3, 1–6.
Viele, G.W., 1973. Structure and Tectonic History of the Ouachita Mountains, Arkansas. In: DeJong, K.A., Scholten, R. (Eds.), Gravity and Tectonics. John Wiley & Sons, New York, pp. 361–377.
Viele, G.W., 1989. The Ouachita Orogenic Belt. In: Hatcher, R.D., Thomas, W.A., Viele, G.W. (Eds.), The Appalachian-Ouachita Orogen in the United States. DNAG, the Geology of North America F-2. Geological Society of America, Boulder, Colorado, pp. 555–561.
Watson, E.B., Liang, Y.A., 1995. A simple model for sector zoning in slowly grown crystals; implications for growth rate and lattice diffusion, with emphasis on accessory minerals in crustal rocks. American Mineralogist 80, 1179–1187.
Watt, G.R., Wright, P., Galloway, S., McLean, C., 1997. Cathodoluminescence and trace element zoning in quartz phenocrysts and xenocrysts. Geochimica et Cosmochimica Acta 61, 4337–4348.
Wiltschko, D.V., Morse, J.W., 2001. Crystallization pressure versus "crack-seal" as the mechanism for banded veins. Geology 29, 79–82.